Reducing Hypermuscularization of the Transitional Segment between Arterioles and Capillaries Protects Against Spontaneous Intracerebral Hemorrhage

Reducing hypermuscularization of the transitional segment between arterioles and capillaries protects against spontaneous intracerebral hemorrhage

Short title: A novel mechanism of intracerebral hemorrhage

Authors

Julien Ratelade, PhD, Nicholas R. Klug, PhD[#], Damiano Lombardi, PhD[#], Monara Kaelle Servulo Cruz Angelim, PhD[#], Fabrice Dabertrand, PhD, Valérie Domenga-Denier, Rustam Al-Shahi Salman, PhD, Colin Smith, MD, Jean-Frédéric Gerbeau, PhD, Mark T. Nelson, PhD, Anne Joutel MD, PhD

# equal contribution

Corresponding author:

Anne Joutel, Inserm UMR 1266, Institute of Psychiatry and Neurosciences of Paris, 102-108 rue de la Santé, 75014 Paris, France

Email: anne.joutel@inserm.fr

Tel: +33 1 40 78 92 96

Text word counts (does not include title, abstract, ref, table, legends): 5151

ABSTRACT

Background: Spontaneous deep intracerebral hemorrhage (ICH) is a devastating subtype of stroke without specific treatments. It has been thought that smooth muscle cell (SMC) degeneration at the site of arteriolar wall rupture may be sufficient to cause hemorrhage. However, deep ICHs are rare in some aggressive small vessel diseases that are characterized by significant arteriolar SMC degeneration. Here we hypothesized that a second cellular defect may be required for the occurrence of ICH.

Methods: We studied a genetic model of spontaneous deep ICH using *Col4a1*$^{+/G498V}$ and *Col4a1*$^{+/G1064D}$ mouse lines that are mutated for the alpha1 chain of Collagen type IV. We performed high resolution imaging and molecular analyses of cerebroretinal microvessels, genetic rescue experiments, vascular reactivity analysis and computational modeling. We also examined post-mortem brain tissues from patients with sporadic deep ICH.

Results: We identified in the normal cerebroretinal vasculature a novel segment between arterioles and capillaries, herein called the transitional segment (TS), that is covered by mural cells distinct from SMCs and pericytes. In *Col4a1* mutant mice, this TS was hypermuscularized, with a hyperplasia of mural cells expressing more contractile proteins, whereas the upstream arteriole exhibited a loss of SMCs. Mechanistically, TS showed a transient increase in proliferation of mural cells during post-natal maturation. Mutant brain microvessels, unlike mutant arteries, displayed a significant upregulation of SM genes and *Notch3* target genes, and genetic reduction of *Notch3* in *Col4a1*$^{+/G498V}$ mice protected against ICH. Retina analysis showed that hypermuscularization of the TS was attenuated but arteriolar SMC loss unchanged in *Col4a1*$^{+/G498V}$, *Notch3*$^{+/-}$ mice. Moreover, hypermuscularization of the retinal TS increased its contractility and tone and raised the intravascular pressure in the upstream feeding arteriole. Consistently, we similarly found

hypermuscularization of the TS and focal arteriolar SMC loss in brain tissues from patients with sporadic deep ICH.

Conclusions: Our results suggest that hypermuscularization of the TS, via increased Notch3 activity, is involved in the occurrence of ICH in *Col4a1* mutant mice, by raising the intravascular pressure in the upstream feeding arteriole and promoting its rupture at the site of SMC loss. Our human data indicate that these 2 mutually reinforcing vascular defects may represent a general mechanism of deep ICH.

Clinical Perspective

What is new ?

- *Col4a1* mutant mice, a genetic model of spontaneous deep intracerebral hemorrhage (ICH), exhibit excessive muscularization of the transitional segment (TS) at the interface between arterioles and capillaries, as a result of increased Notch3 activity, in addition to focal loss of smooth muscle cells in arterioles, in the brain and the retina.
- Genetic reduction of *Notch3* in *Col4a1* mutant mice protects against ICH.
- Analysis of the retinal vasculature supports the concept of 2 mutually reinforcing vascular defects as a mechanism of deep ICH, in which hypermuscularization of TS raises the intravascular pressure in the upstream feeding arteriole crippled by smooth muscle cell loss, and this ultimately leads to arteriolar rupture.

What are the clinical implications?

- Spontaneous ICH accounts for 10-20% of all strokes and is the most devastating subtype of stroke, without specific treatments.
- Because these 2 mutually reinforcing vascular defects are present in the brain of patients with sporadic deep ICH, this may represent a general mechanism of deep ICH and a putative therapeutic target.

INTRODUCTION

Spontaneous (non-traumatic) intracerebral hemorrhage (ICH) accounts for 9-27% of all strokes[1], causing about 3 million cases worldwide per year[2]. This stroke subtype is the most devastating one because it is associated with high mortality rates (55% at one year) and major permanent disabilities in patients who survive[3,4]. Cerebral small vessel diseases underlie the vast majority of ICHs[5]: so-called hypertension-related arteriopathy accounts for almost all deep ICH (occurring in the basal ganglia, thalamus, cerebellum or brainstem), whereas just over half of lobar ICH is associated with cerebral amyloid angiopathy. Importantly, as population blood pressure control has improved, epidemiological studies have found a decreasing prevalence of uncontrolled hypertension at the time of ICH diagnosis[6,7], yet ICH incidence appears unchanged[3].

Pathological studies on postmortem human brains have suggested that deep ICH results from focal smooth muscle cell (SMC) degeneration in the media of cerebral arterioles and replacement with collagen, which is structurally stiff and brittle[8–10]. It has been speculated that the weakened arteriole dilates and eventually bursts at bifurcation sites and that this occurs preferentially in deep brain regions where penetrating arterioles are exposed to high perfusion pressure due to their proximity to the circle of Willis[11]. However, SMC loss alone may not be sufficient to cause ICH because deep ICHs are rare in some aggressive small vessel diseases that are characterized by significant arteriolar SMC degeneration[12]. Emerging evidence indicates that mural cells exhibit a variety of cell phenotypes along the microvascular tree[13], raising the possibility that mural cells may respond in different ways to the factors underlying the arteriopathy.

Animal models of spontaneous deep ICHs are very rare. Beside sporadic forms of deep ICH, monogenic forms largely indistinguishable from sporadic forms have been characterized offering excellent opportunities for mechanistic studies using genetic models. Heterozygous

mutations in the α1 (COL4A1) chain of collagen type IV, which is a major component of vascular basement membranes (BM), are associated with spontaneous deep ICHs in humans or mice in the absence of hypertension, although with incomplete penetrance [14,15].

Herein, we hypothesized that a second cellular defect may be required for the occurrence of ICH and we used *Col4a1* mutant mice to test this hypothesis.

METHODS

The data that support the findings of this study are available from the corresponding author upon reasonable request.

Human tissue samples

Post-mortem frozen and paraffin embedded human brain samples were obtained from the UK Medical Research Council Brain Bank of the University of Edinburgh, with informed consent from patients or their families for their inclusion in the Lothian IntraCerebral Haemorrhage, Pathology, Imaging and Neurological Outcome (LINCHPIN) study[5]. The use of postmortem brain tissues for research was approved by the Institutional Review Board of INSERM (IRB00003888, n°17-392).

Mice

Col4a1$^{+/G498V}$ mice used in this study were generated on a mixed 50% C57BL/6 – 50% 129/Sv background as described previously[14,16]. *Col4a1*$^{+/G1064D}$ mice on a C57BL/6 background were obtained from GlaxoSmithKline (Brentford, UK). *Notch3*$^{+/-}$ mice were described previously[17] and maintained on a 129/Sv background. All animals were randomized for their genotype information and were included in the study. Mice were maintained in a specific pathogen-free environment. Experiments were conducted in accordance with the guidelines of our local institutional Animal Care and Use Committee (Lariboisiere-Villemin, CEA9).

All other methods are described in the supplementary material.

Statistical analysis

Unless specified otherwise, data in figures and text are presented as means ± standard deviation. Statistical significance was determined using either two-tailed Student's t-test, two-tailed Mann-whitney test, one-way analysis of variance (ANOVA) followed by Tukey's post hoc test, 2-way ANOVA followed by Bonferroni post hoc test or Kruskal-Wallis test followed

by Dunn's post hoc test, as specified in figure legends (GraphPad Prism 7 software). For large samples (n>8), data were analyzed using parametric or non-parametric tests depending on the result of the D'Agostino-Pearson omnibus normality test. Chi-square test was used to compare the penetrance of ICHs between different groups.

RESULTS

An unbiased, marker-based mural cell characterization of the retinal vasculature

We focused on the superficial retinal vascular network that exhibits many similarities with the cerebral vasculature and offers the advantage of being nearly planar on flat-mounted retina preparations and highly stereotyped (Fig 1A). Moreover, we recently established the validity of the retinal vasculature as a study model in the COL4A1 disease[14]. Flat-mounted retinas of adult mice were stained for various mural cell markers including smooth muscle contractile proteins —α smooth muscle actin (α-SMA) or smooth muscle myosin heavy chain (SMMHC)—, the intermediate filament protein desmin, the plasma membrane chondroitin sulfate proteoglycan (NG2), Platelet-derived growth factor receptor-beta (PDGFR-β), or aminopetidase N (CD13). Markers of endothelial cells (VE-cadherin), astrocytes (GFAP, aquaporin 4), BM (perlecan, COL4A2) or elastic lamina (elastin or Alexa Fluor 633–conjugated hydrazide[18]) were also used. Arterioles (average diameter 26 µm) were surrounded by α-SMA^{high}, SMMHC^{high}, desmin^{low}, CD13^{low}, NG2^{low} and PDGFR-β^{low} SMCs. Here, SMCs had a flat ring-shape and were circumferentially organized in a perpendicular manner towards the vessel axis (Figs 1B, S1 and S2). Veins (average diameter 32 µm) were surrounded by stellate-shaped α-SMA^{low}, SMMHC^{low}, desmin^{high}, CD13^{low}, NG2^{low} and PDGFR-β^{high} SMCs (Figs 1B, S1 and S2). Capillaries (average diameter 4.1 µm) were covered by α-SMA^{negative}, SMMHC^{negative}, desmin^{high}, CD13^{high}, NG2^{high} and PDGFR-β^{high} mural cells, hereafter called pericytes, showing a protruding ovoid cell body ("bump on a log") embedded in the BM, and elongated thin processes (Figs 1B, S1 and S2). Interestingly the vascular segment located between arterioles and capillaries (average diameter 10 µm) was covered by distinct mural cells, expressing both arteriolar SMC and pericyte markers. Namely these cells were α-SMA^{high}, SMMHC^{high}, desmin^{high}, CD13^{high}, NG2^{high} and PDGFR-β^{high}. These mural cells had a pericyte-like protruding cell body, which contained the nucleus and

where NG2 staining was mostly concentrated (Fig S2B), but larger and irregular ensheathing processes projecting orthogonally over the vessel, bright for α-SMA and SMMHC (Figs 1B, S1 and S2). Thereafter, this vascular segment will be referred as "the transitional segment" (TS) and its mural cells as "transitional cells". TS were present at every arteriole/capillary transition, usually at the 1^{st}-3^{rd} branch orders (0 being the proximal arteriole starting in the center of the retina) (Fig S3). Interestingly, TS, unlike arterioles, were devoid of elastic fibers (Fig. S4C-D). On the other hand, expression of VE-cadherin, perlecan, COL4A2, GFAP and aquaporin 4 was almost comparable along the arteriovenous bed (Fig. S4 and data not shown).

Col4a1$^{+/G498V}$ mice have hypermuscularized TS in addition to arteriolar SMC loss in the retinal vasculature

Next, we studied microvascular changes in the retina of adult *Col4a1$^{+/G498V}$* mice (6-month-old). Our previous work had shown segmental and focal loss and apoptosis of SMCs in the retinal arterioles, starting from 3 months of age[14]. In keeping with this finding, we observed that mural cell loss was strictly restricted to retinal arterioles and that remaining SMCs stained negative for NG2 and low for desmin, suggesting that mutant SMCs have not undergone a phenotypic switch towards a transitional cell or pericyte phenotype (Fig. S5). In striking contrast, mutant TS exhibited a significantly higher number of mural cells with an increased expression of contractile proteins including α-SMA or SMMHC (Fig. 2 A-C) that was already present at one month of age (Fig S6), and we coined the term "hypermuscularization" to designate these alterations. On the other hand, cell density and phenotype of pericytes were unchanged in mutant capillaries although pericyte coverage was slightly increased (Fig. S7) and no overt anomalies of SMCs were noticed in mutant veins.

To delineate the underlying cellular mechanisms of TS pathology, we examined whether there was abnormal mural cell proliferation or apoptosis in mutant mice. The vascularization of the murine retina occurs after birth and prior works suggest that mural cells are derived from a

common NG2+ precursor cell already present at birth[19,20]. At post-natal day 10 (P10), arterioles were already easily recognizable as α-SMA bright vessels, yet SMCs were still NG2 bright and had a protruding cell body, whereas TS just started to become discernable (Figs 2D and S8). At P10, TS consisted in small branches covered by rounded mural cells that were NG2 bright and α-SMA low-to-very pale (white-boxed area in Fig. 2D). We found that the length and α-SMA expression level of TS were comparable between wildtype and mutant mice (Fig. 2F). Incorporation of 5-ethynyl-2'-deoxyuridine (EdU) revealed a low number of proliferating mural cells in TS, but which was significantly higher in *Col4a1*$^{+/G498V}$ mice (Fig. 2D-F). Very few apoptotic mural cells were present in TS in wildtype and mutant mice (Fig S8D). At P23, TS had further grown and almost reached the adult mature state described above. The length of TS was comparable between wildtype and mutant mice but α-SMA expression level was significantly increased in mutant mice. Proliferating mural cells were no longer detected and almost no apoptotic mural cells were observed in *Col4a1*$^{+/+}$ and *Col4a1*$^{+/G498V}$ mice (Fig S8). SMC proliferation or apoptosis in arterioles was also very low at P10 and P23, and notably comparable between wildtype and mutant mice (Fig. S8).

The brain vasculature of Col4a1$^{+/G498V}$ and Col4a1$^{+/G1064D}$ mutant mice display similar hypermuscularization of TS in addition to arteriolar SMC loss

We next assessed whether the brain vasculature of *Col4a1* mutant mice displayed similar changes to those of the retinal vasculature. Immunostaining of thick (100µm) brain slices indicated that brain arterioles, like retinal arterioles, were surrounded by α-SMA^{high} , desmin^{low} and NG2^{low} SMCs, forming narrow circumferential bands, and brain TS were surrounded by α-SMA^{high} , desmin^{high} and NG2^{high} mural cells having larger and irregular ensheathing processes and a protruding cell body containing the nucleus wrapped by a bright NG2 staining (Figs 3A-B and S9). Consistent with our previous work[14], we detected in

Col4a1$^{+/G498V}$ mice focal and segmental loss of SMCs in penetrating arterioles within regions prone to ICH, like the thalamus (data not shown). Importantly, we found that α-SMA expression in TS was significantly increased in *Col4a1*$^{+/G498V}$ mice compared to *Col4a1*$^{+/+}$ mice, not only in the thalamus but also in other brain regions, such as the cortex and striatum, that are spared by ICH (Fig 3C-D).

The combination of arteriolar SMC loss and hypermuscularization of TS was similarly observed in *Col4a1*$^{+/G1064D}$ mice, another independent *Col4a1* mutant line [21–23] in both the retina and the brain, although vascular pathology was more severe than in *Col4a1*$^{+/G498V}$ mice (expanded results, Figs S10-S11).

To understand the reason behind the differences between TS and arterioles in mutant mice, and because Col4a1 mutations have been shown to decrease COL4 expression[14], we asked whether COL4 expression levels were different between mutant arterioles and TS. Brain cryosections (20µm-thick) of *Col4a1*$^{+/+}$ and *Col4a1*$^{+/G498V}$ mice were immunostained with a monoclonal antibody specific for COL4A2, which assembles with COL4A1 to form the COL4A1A1A2 heterotrimer. Remarkably, COL4A2 immunoreactivity was significantly decreased in mutant TS but unchanged in mutant arterioles (Fig. S12).

In the ensuing study, we focused on the role of the hypermuscularization of TS in ICH.

Expression of SMC genes and Notch3 target genes is upregulated in Col4a1$^{+/G498V}$ brain microvessel preparations enriched in TS

To investigate molecular changes occurring in TS, we purified brain microvessels from *Col4a1*$^{+/+}$ and *Col4a1*$^{+/G498V}$ mice using sequential filtrations through nylon meshes of decreasing pore sizes. Immunostaining of brain vessels retained on the 100 µm-nylon mesh mainly comprised arterioles and veins (Fig 4A, top panel) whereas the 40 µm-retentate was

enriched in TS, and also in capillaries (Fig 4A, bottom panel). We found that genes coding for the contractile proteins α-SMA and SMMHC were significantly upregulated in the TS enriched fraction of *Col4a1*$^{+/G498V}$ mice, as well as genes coding for desmin, the actin-binding proteins calponin and SM22 and the transcription factor myocardin, suggesting an increased differentiation of mural cells (Fig 4B).

The Notch3 receptor is predominantly expressed in vascular SMCs and Notch3 signaling pathway plays a pivotal role in the development and maturation of blood vessels[24]. Moreover, recent work suggests that activation of the Notch3 pathway promotes pulmonary arterial hypertension by stimulating SMC proliferation and muscularization of small pulmonary arteries[25]. Given these observations, and the finding that Notch3 is also expressed in transitional cells (Fig. S13), we suspected that hypermuscularization of the TS could be mediated by a dysregulation of the Notch3 pathway, and thus we quantified the expression of target genes regulated by Notch3[26,27] (Supplementary table 1). Because our brain microvessel preparations also contained endothelial cells, we selected Notch3 target genes that were expressed exclusively in mural cells according to previous works[26,27] or single cell RNAseq analysis of mouse brain microvessels (*http://betsholtzlab.org/VascularSingleCells/database.html*) [13]. We found that 7 out of 11 of these Notch3 target genes were upregulated in brain microvessels of *Col4a1*$^{+/G498V}$ mice (Fig. 4C). In striking contrast, expression level of SM marker genes was essentially unchanged in dissected brain arteries of *Col4a1*$^{+/G498V}$ mice and only 2 out of 11 of Notch3 target genes were upregulated in mutant brain arteries (Fig. 4D,E). Altogether, our results suggest that the increased muscularization of mutant TS arises from an increased activation of Notch3 pathway.

Genetic reduction of Notch3 in Col4a1$^{+/G498V}$ mice attenuates the hypermuscularization of TS in the retina and protects against ICH

To confirm that activation of the Notch3 pathway contributed to the hypermuscularization of TS and assess whether this hypermuscularization was involved in ICH in *Col4a1* mutant mice, we adopted a genetic interaction approach. To avoid confounding effects induced by the complete loss of Notch3, which causes prominent loss of SMCs[17,28,29], we generated and analyzed *Col4a1*$^{+/G498V}$ lacking 1 allele of Notch3, along with their control littermates, at 6 months of age. Loss of a single allele of Notch3 in wildtype mice (*Notch3*$^{+/-}$) has no detectable morphological effect on the retinal microvasculature[29] but significantly reduces Notch3 activity [26]. Genetic reduction of Notch3 in *Col4a1* mutant mice (*Col4a1*$^{+/G498V}$, *Notch3*$^{+/-}$) had no significant effect on SMC loss in retinal arterioles (Fig. 5A,B), however, it strikingly significantly attenuated α-SMA expression and mural cell number in TS (Fig 5C,D). Remarkably, the mean number of ICH was significantly reduced in *Col4a1*$^{+/G498V}$, *Notch3*$^{+/-}$ mice compared to *Col4a1*$^{+/G498V}$, *Notch3*$^{+/+}$ mice (Fig 5E,F). Moreover, the penetrance of ICH was drastically reduced in *Col4a1*$^{+/G498V}$, *Notch3*$^{+/-}$ mice, with ICH being detected in only 20% of mice compared to near 60% in the *Col4a1*$^{+/G498V}$, *Notch3*$^{+/+}$ group (*P*=0.024 by the Chi-square test)..

Mutant TS are more contractile in response to thromboxane receptor agonist and increased intraluminal pressure

To pinpoint the mechanism by which hypermuscularization of the TS contributed to the occurrence of ICH, we next performed functional studies. To achieve this, we used the retina where TS can be easily identified *ex vivo* under phase contrast microscopy (Fig S3). To study vascular responses closest to physiological conditions, we developed an *ex vivo* pressurized retina preparation (Fig 6A). We assessed the response of TS to two standard vasoconstrictors, KCl and the thromboxane mimetic U-46619 on retina explants from *Col4a1*$^{+/+}$ and *Col4a1*$^{+/G498V}$ mice aged 6 months (Fig. 6B and supplementary Table 2). Addition of 60 mM KCl to the superfusion chamber elicited a robust and quick constriction of wildtype TS, with a

trend toward a stronger constriction in *Col4a1*$^{+/G498V}$ vessels (Fig S14). U-46619 (10-100nM) produced a concentration-dependent constriction of TS that was significantly increased in *Col4a1*$^{+/G498V}$ mice at 50 nM (36% diameter reduction in mutant mice versus 3% in control mice) (Fig 6C,D). We also examined the contractile response of TS to increased intraluminal pressure. Both *Col4a1*$^{+/+}$ and *Col4a1*$^{+/G498V}$ TS decreased luminal diameter in response to the pressure change, however *Col4a1*$^{+/G498V}$ TS exhibited a ~5.5-fold greater constriction than *Col4a1*$^{+/+}$ TS (Fig. 6E-F).

Hypermuscularization of the TS cripples the pressure drop in the microvasculature

We then hypothesized that the higher tone and contractility of mutant TS could compromise the pressure drop along the microvasculature. An abnormally higher intravascular pressure at the level of arterioles combined with SMC loss might favor their rupture. Measuring intravascular pressure *in vivo* in the microvasculature is extremely challenging and yet limited to larger vessels. Moreover, assessing the pressure drop along the microvascular bed would require several measurements at different locations which is not feasible *in vivo*. Therefore, we used computational modeling to simulate the pressure distribution in different parts of the microvasculature in the retina. We used an established mathematical model of an artery/arteriolar human retinal network in which mural cells are implemented as fibers in the vascular wall[30,31] (Fig. 7A). In *Col4a1* mutant mice, density of mural cells was decreased in arterioles to model SMC loss and increased in TS to simulate the hypermuscularization (Fig. 7B). Measurements of systolic and diastolic blood pressures by tail-cuff plethysmography showed a 11% decrease in *Col4a1* mutant mice (Fig. S15). Hence, blood pressures at the entry of the retinal vascular network were decreased proportionally in *Col4a1* mutant mice and used as input parameters for the model (Fig. 7B). Intravascular pressure was then simulated in control and mutant mice all along the arterioles and TS (Fig. 7C). Fig 7D shows the values of systolic and diastolic intravascular pressures in 10 different locations during a

typical cardiac cycle. In control mice, pressure continuously dropped from 40 to 20 mmHg. In *Col4a1* mutant mice, a lower pressure was observed in proximal arterioles (positions 1-3) due to the slight systemic hypotension. However, pressure drop was reduced resulting in higher intravascular pressure in middle-size arterioles (positions 4-8) and TS (positions 9-10) compared to controls. Moreover, in this part of the vascular network the pulse pressure (difference between the systolic and diastolic pressure) was larger in *Col4a1* mutant mice. Thus, these data suggest that the hypermuscularization of TS leads to an abnormally elevated mean and pulse pressure in the feeding upstream arteriole.

Diffuse mural cell loss is not associated with ICH

Our findings above predict that, conversely, loss of transitional cells in TS in addition to SMC loss in arterioles should not lead to ICH (Fig. 7E). Consistent with previous reports[17,28,29], cerebral and retinal arterioles of mice completely lacking *Notch3* exhibited prominent SMC loss (Figs S16-S17). However, unlike *Col4a1* mutant mice, we found that TS in *Notch3*$^{-/-}$ mice also showed dramatic loss of transitional cells in both the retina and the brain (Figs S16-S17). Computational modeling revealed that arterioles in *Notch3*$^{-/-}$ mice were exposed to lower intravascular pressure compared to controls (Fig. 7C,D). Remarkably, Perl's staining revealed no ICH in *Notch3*$^{-/-}$ mice aged 10-12 months (Fig. S17).

Cerebral TS are hypermuscularized in humans with sporadic deep ICH

Finally, we tested if hypermuscularization of TS was also present in humans with sporadic ICH. Similarly to murine cerebral vessels, human cerebral arteries were surrounded by flat ring-shaped SMCs whereas α-SMA positive smaller vessels (diameter between 5 and 15 µm) were covered by mural cells having a protruding ovoid cell body (Fig. S18). These vessels are most likely TS, although transitional cells could not be further characterized because none of the antibodies against NG2, desmin or aminopeptidase N worked on human post-mortem

brain tissue in our experimental conditions. To assess vascular remodeling in human deep ICH, we immunostained for α-SMA paraffin sections of postmortem brain tissues from adults who suffered from spontaneous deep ICH (Fig. 8A) and age and sex-matched control subjects (Supplementary table 3). To ensure that vascular lesions were not secondary to ICH, we used tissue sampled in the hemisphere contralateral to the hemorrhage, and we analyzed sections through the basal ganglia. In agreement to what has been previously reported[8], we observed that some, but not all, arteries in patients had a markedly reduced α-SMA staining in the media with an uneven distribution of stained SMC, consistent with segmental and focal SMC degeneration (Fig. S19). In contrast, TS in ICH patients often showed a marked increased immunostaining for α-SMA compared to controls, suggesting an increased number or hypertrophy of mural cells (Fig 8B). We imaged cross-sectional profiles of 525 randomly selected TS/arterioles in patients and controls. Quantification of the ratio of the area stained for α-SMA (media) over the area of the lumen confirmed that α-SMA staining was significantly thicker in TS (lumen diameter between 5 and 15 µm) from ICH patients whereas α-SMA staining in arterioles (lumen diameter > 15µm) was comparable between ICH patients and controls (Fig. 8C-D). Overall, our data suggest that hypermuscularization of TS is a common pathological mechanism in spontaneous deep ICH.

DISCUSSION

In the present study, we investigated the microvascular pathology in mice mutant for collagen type IV, a model of hereditary spontaneous deep ICH, and provided strong experimental evidence for two mutually-reinforcing defects of the brain microvasculature as a new mechanism for ICH. In our previous study, we had demonstrated that ICH originate from deep brain arteries with focal and segmental loss of SMC[14]. In the present study, we demonstrate that TS, the downstream microvessels at the interface between arteries and capillaries, show an exaggerated muscularization with higher contractility and tone. Our data support a mechanism in which hypermuscularization of mutant TS is driven by increased Notch3 activity, cripples the pressure drop along the arterio-capillary axis, raising the intravascular pressure in the upstream feeding arteriole and promoting its rupture at the site of SMC loss (Fig. 7E). We found similar microvascular lesions in post mortem brain tissues from patients with sporadic deep ICH, indicating that this may represent a general mechanism of deep ICH.

Zonation of microvascular pathology in Col4a1-related small vessel disease

Several groups have highlighted the diversity of mural cells in the brain microvasculature as arterioles branch into capillaries based on cellular morphology, α-SMA content or vascular territory[32,33]. Recently, Vanlandewijck, He and colleagues proposed the concept of mural cell zonation, by which these cells can be grouped in distinct populations according to their gene repertoire[13]. Herein, we took advantage of the flat mounted retina preparation, in which the arteriovenous axis can be observed in a single plane, to precisely define the phenotype of mural cells at the arteriole-capillary interface, by using a combination of several mural cell markers and high-resolution imaging. Consistent with recent reports[32,33], we found that

microvessels at the interface between arterioles and capillaries (mean diameter 10 μm), herein called TS, are covered by a population of mural cells that are distinct from the canonical ring-shaped α-SMA positive SMCs located in arterioles and arteries, and the canonical α-SMA negative pericytes, which have a protruding cell body and extend thin and long processes along the capillaries. We further established that these mural cells robustly express markers of both canonical SMCs and pericytes and extend large and short processes but have a protruding cell body. We then demonstrated the presence of similar transitional cells in the cerebral vessels. We believe that the name of transitional cell, rather than "contractile pericyte" [34,35], "ensheathing pericyte"[32] or "pre-capillary SMC"[33] better reflects the similarity and the continuum between these mural cells and the adjacent canonical SMCs and pericytes.

Remarkably, the zonation of mural cells, as described above, coincides with the zonation of microvascular pathology in *Col4a1* mutant mice. Notably, our time course, cellular, molecular and genetic experiments strongly suggest that the exaggerated muscularization of the TS and arteriolar SMC loss are driven by different mechanisms.

Mechanism of excessive muscularization of TS in *Col4a1* mutant mice

Increased α-SMA expression and mural cell numbers in TS include several possible underlying mechanisms. Analysis of the retinal vasculature at P10, the earliest time point when TS were discernable, revealed that proliferation of mural cells, although low, was transiently increased in mutant TS. While the increased number of transitional cells may largely contribute to the increased expression of SM contractile proteins, our finding of an upregulation of several SM genes including myocardin, a transcription factor critically involved in SMC differentiation, is consistent with an enhanced differentiation of transitional cells in mutant TS— noting that we did not find evidence of a premature differentiation of these cells.

Our findings that Notch3 target genes were upregulated in mutant brain microvessels and that hypermuscularization of retinal TS in *Col4a1*$^{+/G498V}$ mice was attenuated by genetic reduction of Notch3, suggest that increased Notch3 activity is a driver of TS pathology. This conclusion is consistent with a number of previous studies that clearly established a pivotal role of Notch3 on early mural cell specification, differentiation and expression of SMC genes[17,28,29,36–38]. It is also worth mentioning that Notch3 has been identified as a mediator of SMC proliferation and muscularization of small pulmonary arteries in the context of pulmonary hypertension[25]. Considering a recent report showing that COL4 can repress Notch3 signaling[39], it is plausible that the reduction in COL4 expression in mutant TS could be involved in this increased Notch3 activity. Nevertheless, further studies are warranted to better understand the mechanisms by which Col4a1 mutations increase Notch3 activity in mutant TS and of Notch3-mediated hypermuscularization of mutant TS. In this regard, it will be critical to better understand the molecular and physiological factors that underlie the differentiation of mural cells in transitional or arteriolar vessels. However, one current limitation is the absence of specific marker or genetically encoded reporter of transitional cells.

Why TS respond to Col4a1 mutations with hypermuscularization whereas arteries do not?

We found that arteries differed from TS in several respects. Notably, Col4a1 mutation did not affect expression of COL4 and marginally affected expression of Notch3 target genes in mutant arteries. This different response of arterial SMCs and transitional cells to Col4a1 mutation may originate from their distinct intrinsic molecular identity highlighted in this study. Furthermore, the distinct environment of SMCs in arterioles compared to mural cells in transitional segments offers an additional possible explanation. Indeed, communication

between endothelial cells and SMCs in arteries is hampered by the presence of an internal elastic lamina which restricts cell-cell communication to myoendothelial projections [40]. In contrast, endothelial cells are in direct contact with transitional cells in TS, which are devoid of elastic lamina. Thus, the distinct pathology of arteriolar SMCs and transitional cells in *Col4a1* mutant mice may arise from cell autonomous effects versus endothelial cell-mediated, i.e. non-cell autonomous, effects respectively[41]. Future work is needed to investigate this hypothesis.

Two mutually-reinforcing defects of the brain microvasculature as a key mechanism for spontaneous deep ICH

We recently reported that *Col4a1* mutant mice exhibited arteriolar SMC loss in the brain and the retina, and that ICH originated from arterioles with severe loss of SMC[14]. In this study, we demonstrated that mutant TS in the brain and the retina were hypermuscularized. Our Notch3 genetic reduction experiment in *Col4a1* mutant mice further suggests that hypermuscularization of the TS plays a role in the occurrence of ICH. By analyzing the retina, which is a tractable central nervous system preparation where vessels of the superficial layer are at similar depths and can be easily fully imaged, we demonstrated that hypermuscularization of TS was attenuated and arteriolar SMC loss unchanged in *Col4a1* mutant mice haploinsufficient for *Notch3*. Remarkably, these mice were protected against hemorrhage. Additional studies would be desirable to confirm that hypermuscularization of TS is similarly attenuated and arteriolar SMC loss similarly unchanged in the brain of *Col4a1* compound heterozygotes, although such quantifications are still extremely challenging because the cerebral vasculature spans several spatial scales and forms a highly complex network. Moreover, our demonstration in Notch3 null mice that a severe loss of mural cells in both arterioles and TS does not necessarily lead to ICHs, lends further support to the concept

that the hypermuscularization of TS in addition to arteriolar SMC loss is involved in ICH occurrence.

Hypermuscularization of TS is predicted to locally decrease vessel diameter, increase vascular resistance and raise the intravascular pressure in the upstream proximate arteriole, hence favoring its rupture at the site of SMC loss. Both our experimental data and our computational modeling support these predictions. First, using our pressurized retina preparation, we found that pressure increase caused a significantly higher reduction in the diameter of TS in *Col4a1* mutant mice compared to control mice. Second, our computational modeling revealed that the pressure drop along the arterio-TS axis was crippled in *Col4a1* mutant mice, ie with an abnormally higher intravascular pressure in the proximate feeding arteriole, despite the fact that *Col4a1* mutant mice were slightly hypotensive. Notably, our computational modeling approach showed that arterioles in *Notch3* null mice were instead exposed to lower intravascular pressure, which likely protected them against rupture and hemorrhage as observed experimentally.

ICHs in *Col4a1* mutant mice preferentially occur in the deep parts of the brain. This anatomical specificity of ICH is likely attributed in part to the following factors. First, in a previous study, we reported that arteriolar SMC loss predominated in the deep penetrating arteries[14]. Secondly, although hypermuscularization of TS is not restricted to ICH prone regions, the mechanism by which it favors arteriolar rupture, namely by raising the intravascular pressure at the site of SMC loss, suggests that it could contribute to the regional specificity of ICH. Indeed, recent computational modeling in human suggests that intravascular pressure at the level of perforating arteries in the deep parts of the brain is higher than the one at the level of penetrating arteries in the cortex, owing to their anatomical proximity to the circle of Willis[42]. Therefore, it is anticipated that it is in those deep

penetrating arteries that hypermuscularization of TS should produce the highest local elevation of intravascular pressure.

Excessive muscularization of the TS in sporadic deep ICH

In patients with sporadic deep ICH, SMC degeneration has been documented at the presumed site of arterial wall rupture for many years[10,11]. So far, the assumption has been made that vessel wall degeneration was uniquely responsible for bleeding. Our findings in *Col4a1* mutant mice, a genetic model of spontaneous deep ICH, prompted us to test the possibility that sporadic deep ICH in humans may also arise from a similar zonation of microvascular pathology. Remarkably, analysis of human post-mortem brain tissues from patients with spontaneous deep ICH revealed, in addition to segmental SMC degeneration in arteries, a thickening of α-SMA staining in smaller vessels, consistent with a hyperplasia or hypertrophy of mural cells. Although, we could not unequivocally identify these vessels as TS because most of the mural cell markers used in the mouse did not work on human tissues in our experimental conditions, the presence of protruding cell nuclei and the internal diameter of the affected vessels, comprised between 5-15 µm, strongly suggest that these are TS. Hence our data suggest that the mechanism of ICH identified in *Col4a1* mutant mice also operates in human sporadic deep ICH. Yet, whether Notch3 activity is similarly increased in TS in patients needs to be further investigated.

Our findings open new opportunities towards the development of preventive therapies for ICH. Although several studies have established the benefit of blood pressure lowering in preventing the recurrence of ICH (secondary prevention) [43–45], our data suggest that pharmacological compounds targeting hypermuscularization of the TS may be more effective for both primary and secondary prevention of ICH. Notably, hypermuscularization of the TS may prove to be more easily druggable than arteriolar SMC loss.

Conclusion

Collectively our work is consistent with the new concept of two mutually-reinforcing defects of the brain microvasculature, with arteriolar SMC loss and exaggerated muscularization of the TS, as a new mechanism underlying hereditary and sporadic deep ICH. Hypermuscularization of this segment may represent a novel therapeutic target for ICH prevention.

ACKNOWLEDGEMENTS

We thank the adults included in the LINCHPIN study, and their relatives and carers. Confocal images were acquired at the ImagoSeine (Jacques Monod Institute) and Neurimag (Institute of Psychiatry and Neuroscience of Paris) facilities. The SP8 confocal microscope (Institute of Psychiatry and Neuroscience of Paris) was funded by a grant from Fondation Leducq.

SOURCES OF FUNDING

This work was supported by Fondation Leducq (Transatlantic Network of Excellence on the Pathogenesis of Small Vessel Disease of the Brain) to AJ and MTN, the European Union (Horizon 2020 Research and Innovation Programme SVDs@target under the grant agreement n° 666881), the French National Agency of Research (ANR I-Can) and the French Fondation for Rare Diseases to AJ, the National Institute of Neurological Disorders and Stroke (NINDS) and National Institute of Aging (NIA) (R01NS110656), the National Institutes of Health under Award Number R35HL140027 and the Henry M. Jackson Foundation for the Advancement of Military Medicine (HU0001-18-2-0016) to MTN. The LINCHPIN study was funded by UK Medical Research Council (MRC) and The Stroke Association. The Edinburgh Brain Bank, part of the MRC UK Brain Bank Network, curates the brain tissue from LINCHPIN study tissue donors and controls who died suddenly from non-neurological conditions. The Edinburgh Brain Bank is funded by both MRC and The Stroke Association.

DISCLOSURES

None.

SUPPLEMENTAL MATERIALS

Expanded Material & Methods

Online Figures 1-19

Online Tables I-III

References 46-51

AFFILIATIONS

From Institute of Psychiatry and Neurosciences of Paris, INSERM UMR1266, Paris Descartes University, Paris, France (JR, VDD, MKSCA, AJ); Department of Pharmacology, College of Medicine, University of Vermont, Burlington, VT, USA (NK, FD, MTN, AJ); Inria Paris, Sorbonne Université, Laboratoire Jacques-Louis Lions, Paris, France (DL, JFG) ; Centre for Clinical Brain Sciences, University of Edinburgh, Edinburgh, UK (RA-SS, CS); Division of Cardiovascular Sciences, University of Manchester, Manchester, UK (MTN); DHU NeuroVasc, Sorbonne Paris Cité, Paris, France (AJ)

# Equal contribution (DL, NK, MKSCA)

REFERENCES

1. Feigin VL, Lawes CMM, Bennett DA, Barker-Collo SL, Parag V. Worldwide stroke incidence and early case fatality reported in 56 population-based studies: a systematic review. *Lancet Neurol*. 2009;8:355–369.

2. Feigin VL, Krishnamurthi RV, Parmar P, Norrving B, Mensah GA, Bennett DA, Barker-Collo S, Moran AE, Sacco RL, Truelsen T, Davis S, Pandian JD, Naghavi M, Forouzanfar MH, Nguyen G, Johnson CO, Vos T, Meretoja A, Murray CJL, Roth GA, GBD 2013 Writing Group, GBD 2013 Stroke Panel Experts Group. Update on the Global Burden of Ischemic and Hemorrhagic Stroke in 1990-2013: The GBD 2013 Study. *Neuroepidemiology*. 2015;45:161–176.

3. van Asch CJ, Luitse MJ, Rinkel GJ, van der Tweel I, Algra A, Klijn CJ. Incidence, case fatality, and functional outcome of intracerebral haemorrhage over time, according to age, sex, and ethnic origin: a systematic review and meta-analysis. *Lancet Neurol*. 2010;9:167–176.

4. Cordonnier C, Demchuk A, Ziai W, Anderson CS. Intracerebral haemorrhage: current approaches to acute management. *Lancet*. 2018;392:1257–1268.

5. Rodrigues MA, Samarasekera N, Lerpiniere C, Humphreys C, McCarron MO, White PM, Nicoll JAR, Sudlow CLM, Cordonnier C, Wardlaw JM, Smith C, Al-Shahi Salman R. The Edinburgh CT and genetic diagnostic criteria for lobar intracerebral haemorrhage associated with cerebral amyloid angiopathy: model development and diagnostic test accuracy study. *Lancet Neurol*. 2018;17:232–240.

6. Lovelock CE, Molyneux AJ, Rothwell PM, Oxford Vascular Study. Change in incidence and aetiology of intracerebral haemorrhage in Oxfordshire, UK, between 1981 and 2006: a population-based study. *Lancet Neurol*. 2007;6:487–493.

7. Samarasekera N, Fonville A, Lerpiniere C, Farrall AJ, Wardlaw JM, White PM, Smith C, Al-Shahi Salman R, Lothian Audit of the Treatment of Cerebral Haemorrhage Collaborators. Influence of intracerebral hemorrhage location on incidence, characteristics, and outcome: population-based study. *Stroke*. 2015;46:361–368.

8. Sutherland GR, Auer RN. Primary intracerebral hemorrhage. *J Clin Neurosci*. 2006;13:511–517.

9. Masawa N, Yoshida Y, Yamada T, Joshita T, Sato S, Mihara B. Morphometry of structural preservation of tunica media in aged and hypertensive human intracerebral arteries. *Stroke*. 1994;25:122–127.

10. Takebayashi S, Kaneko M. Electron microscopic studies of ruptured arteries in hypertensive intracerebral hemorrhage. *Stroke*. 1983;14:28–36.

11. Schlunk F, Greenberg SM. The Pathophysiology of Intracerebral Hemorrhage Formation and Expansion. *Transl Stroke Res*. 2015;6:257–263.

12. Chabriat H, Joutel A, Dichgans M, Tournier-Lasserve E, Bousser M-G. Cadasil. *Lancet Neurol*. 2009;8:643–653.

13. Vanlandewijck M, He L, Mäe MA, Andrae J, Ando K, Del Gaudio F, Nahar K, Lebouvier T, Laviña B, Gouveia L, Sun Y, Raschperger E, Räsänen M, Zarb Y, Mochizuki N, Keller A, Lendahl U, Betsholtz C. A molecular atlas of cell types and zonation in the brain vasculature. *Nature*. 2018;554:475–480.

14. Ratelade J, Mezouar N, Domenga-Denier V, Rochey A, Plaisier E, Joutel A. Severity of arterial defects in the retina correlates with the burden of intracerebral haemorrhage in COL4A1-related stroke. *J Pathol*. 2018;244:408–420.

15. Kuo DS, Labelle-Dumais C, Gould DB. COL4A1 and COL4A2 mutations and disease: insights into pathogenic mechanisms and potential therapeutic targets. *Hum Mol Genet*. 2012;21:R97-110.

16. Chen Z, Migeon T, Verpont M-C, Zaidan M, Sado Y, Kerjaschki D, Ronco P, Plaisier E. HANAC Syndrome Col4a1 Mutation Causes Neonate Glomerular Hyperpermeability and Adult Glomerulocystic Kidney Disease. *J Am Soc Nephrol*. 2016;27:1042–1054.

17. Domenga V, Fardoux P, Lacombe P, Monet M, Maciazek J, Krebs LT, Klonjkowski B, Berrou E, Mericskay M, Li Z, Tournier-Lasserve E, Gridley T, Joutel A. Notch3 is required for arterial identity and maturation of vascular smooth muscle cells. *Genes Dev*. 2004;18:2730–5.

18. Shen Z, Lu Z, Chhatbar PY, O'Herron P, Kara P. An artery-specific fluorescent dye for studying neurovascular coupling. *Nat Methods*. 2012;9:273–276.

19. Hughes S, Chan-Ling T. Characterization of smooth muscle cell and pericyte differentiation in the rat retina in vivo. *Invest Ophthalmol Vis Sci*. 2004;45:2795–2806.

20. Ehling M, Adams S, Benedito R, Adams RH. Notch controls retinal blood vessel maturation and quiescence. *Development*. 2013;140:3051–3061.

21. Van Agtmael T, Schlötzer-Schrehardt U, McKie L, Brownstein DG, Lee AW, Cross SH, Sado Y, Mullins JJ, Pöschl E, Jackson IJ. Dominant mutations of Col4a1 result in basement membrane defects which lead to anterior segment dysgenesis and glomerulopathy. *Hum Mol Genet*. 2005;14:3161–3168.

22. Jones FE, Bailey MA, Murray LS, Lu Y, McNeilly S, Schlötzer-Schrehardt U, Lennon R, Sado Y, Brownstein DG, Mullins JJ, Kadler KE, Van Agtmael T. ER stress and basement membrane defects combine to cause glomerular and tubular renal disease resulting from Col4a1 mutations in mice. *Dis Model Mech*. 2016;9:165–176.

23. Jones FE, Murray LS, McNeilly S, Dean A, Aman A, Lu Y, Nikolova N, Malomgré R, Horsburgh K, Holmes WM, Kadler KE, Van Agtmael T. 4-Sodium phenyl butyric acid has both efficacy and counter-indicative effects in the treatment of Col4a1 disease. *Hum Mol Genet*. 2019;28:628–638.

24. Baeten JT, Lilly B. Notch Signaling in Vascular Smooth Muscle Cells. *Adv Pharmacol*. 2017;78:351–382.

25. Li X, Zhang X, Leathers R, Makino A, Huang C, Parsa P, Macias J, Yuan JX-J, Jamieson SW, Thistlethwaite PA. Notch3 signaling promotes the development of pulmonary arterial hypertension. *Nat Med*. 2009;15:1289–1297.

26. Cognat E, Baron-Menguy C, Domenga-Denier V, Cleophax S, Fouillade C, Monet-Leprêtre M, Dewerchin M, Joutel A. Archetypal Arg169Cys mutation in NOTCH3 does not drive the pathogenesis in cerebral autosomal dominant arteriopathy with subcortical infarcts and leucoencephalopathy via a loss-of-function mechanism. *Stroke*. 2014;45:842–849.

27. Fouillade C, Baron-Menguy C, Domenga-Denier V, Thibault C, Takamiya K, Huganir R, Joutel A. Transcriptome analysis for Notch3 target genes identifies Grip2 as a novel regulator of myogenic response in the cerebrovasculature. *Arterioscler Thromb Vasc Biol*. 2013;33:76–86.

28. Liu H, Zhang W, Kennard S, Caldwell RB, Lilly B. Notch3 is critical for proper angiogenesis and mural cell investment. *Circ Res*. 2010;107:860–70.

29. Henshall TL, Keller A, He L, Johansson BR, Wallgard E, Raschperger E, Mäe MA, Jin S, Betsholtz C, Lendahl U. Notch3 is necessary for blood vessel integrity in the central nervous system. *Arterioscler Thromb Vasc Biol*. 2015;35:409–420.

30. Aletti M, Gerbeau J-F, Lombardi D. A simplified fluid-structure model for arterial flow. Application to retinal hemodynamics. *Computational Methods in Applied Mechanics and Engineering*. 2016;306:77–94.

31. Aletti M, Gerbeau J-F, Lombardi D. Modeling autoregulation in three-dimensional simulations of retinal hemodynamics. *Journal for Modeling in Ophthalmology*. 2016;1:88–115.

32. Grant RI, Hartmann DA, Underly RG, Berthiaume A-A, Bhat NR, Shih AY. Organizational hierarchy and structural diversity of microvascular pericytes in adult mouse cortex. *J Cereb Blood Flow Metab*. 2017;271678X17732229.

33. Hill RA, Tong L, Yuan P, Murikinati S, Gupta S, Grutzendler J. Regional Blood Flow in the Normal and Ischemic Brain Is Controlled by Arteriolar Smooth Muscle Cell Contractility and Not by Capillary Pericytes. *Neuron*. 2015;87:95–110.

34. Attwell D, Mishra A, Hall CN, O'Farrell FM, Dalkara T. What is a pericyte? *J Cereb Blood Flow Metab*. 2016;36:451–455.

35. Hall CN, Reynell C, Gesslein B, Hamilton NB, Mishra A, Sutherland BA, O'Farrell FM, Buchan AM, Lauritzen M, Attwell D. Capillary pericytes regulate cerebral blood flow in health and disease. *Nature*. 2014;508:55–60.

36. Doi H, Iso T, Sato H, Yamazaki M, Matsui H, Tanaka T, Manabe I, Arai M, Nagai R, Kurabayashi M. Jagged1-selective notch signaling induces smooth muscle differentiation via a RBP-Jkappa-dependent pathway. *J Biol Chem*. 2006;281:28555–28564.

37. Granata A, Bernard WG, Zhao N, Mccafferty J, Lilly B, Sinha S. Temporal and embryonic lineage-dependent regulation of human vascular SMC development by NOTCH3. *Stem Cells Dev*. 2015;24:846–856.

38. Ando K, Wang W, Peng D, Chiba A, Lagendijk AK, Barske L, Crump JG, Stainier DYR, Lendahl U, Koltowska K, Hogan BM, Fukuhara S, Mochizuki N, Betsholtz C. Peri-arterial specification of vascular mural cells from naïve mesenchyme requires Notch signaling. *Development*. 2019;146.

39. Zhang X, Meng H, Wang MM. Collagen represses canonical Notch signaling and binds to Notch ectodomain. *Int J Biochem Cell Biol*. 2013;45:1274–1280.

40. Sandow SL, Gzik DJ, Lee RMKW. Arterial internal elastic lamina holes: relationship to function? *J Anat*. 2009;214:258–266.

41. Sheikh AQ, Saddouk FZ, Ntokou A, Mazurek R, Greif DM. Cell Autonomous and Non-cell Autonomous Regulation of SMC Progenitors in Pulmonary Hypertension. *Cell Rep*. 2018;23:1152–1165.

42. Blanco PJ, Müller LO, Spence JD. Blood pressure gradients in cerebral arteries: a clue to pathogenesis of cerebral small vessel disease. *Stroke Vasc Neurol*. 2017;2:108–117.

43. Biffi A, Anderson CD, Battey TWK, Ayres AM, Greenberg SM, Viswanathan A, Rosand J. Association Between Blood Pressure Control and Risk of Recurrent Intracerebral Hemorrhage. *JAMA*. 2015;314:904–912.

44. PROGRESS Collaborative Group. Randomised trial of a perindopril-based blood-pressure-lowering regimen among 6,105 individuals with previous stroke or transient ischaemic attack. *Lancet*. 2001;358:1033–1041.

45. SPS3 Study Group, Benavente OR, Coffey CS, Conwit R, Hart RG, McClure LA, Pearce LA, Pergola PE, Szychowski JM. Blood-pressure targets in patients with recent lacunar stroke: the SPS3 randomised trial. *Lancet*. 2013;382:507–515.

46. Khoshnoodi J, Pedchenko V, Hudson BG. Mammalian collagen IV. *Microsc Res Tech*. 2008;71:357–370.

47. Chen Z-L, Yao Y, Norris EH, Kruyer A, Jno-Charles O, Akhmerov A, Strickland S. Ablation of astrocytic laminin impairs vascular smooth muscle cell function and leads to hemorrhagic stroke. *J Cell Biol*. 2013;202:381–395.

48. Yao Y, Chen Z-L, Norris EH, Strickland S. Astrocytic laminin regulates pericyte differentiation and maintains blood brain barrier integrity. *Nat Commun*. 2014;5:3413.

49. De Silva TM, Faraci FM. Microvascular Dysfunction and Cognitive Impairment. *Cell Mol Neurobiol*. 2016;36:241–258.

50. Rannikmäe K, Davies G, Thomson PA, Bevan S, Devan WJ, Falcone GJ, Traylor M, Anderson CD, Battey TWK, Radmanesh F, Deka R, Woo JG, Martin LJ, Jimenez-Conde J, Selim M, Brown DL, Silliman SL, Kidwell CS, Montaner J, Langefeld CD, Slowik A, Hansen BM, Lindgren AG, Meschia JF, Fornage M, Bis JC, Debette S, Ikram MA, Longstreth WT, Schmidt R, Zhang CR, Yang Q, Sharma P, Kittner SJ, Mitchell BD,

Holliday EG, Levi CR, Attia J, Rothwell PM, Poole DL, Boncoraglio GB, Psaty BM, Malik R, Rost N, Worrall BB, Dichgans M, Van Agtmael T, Woo D, Markus HS, Seshadri S, Rosand J, Sudlow CLM, METASTROKE Consortium, CHARGE WMH Group, ISGC ICH GWAS Study Collaboration, WMH in Ischemic Stroke GWAS Study Collaboration, International Stroke Genetics Consortium. Common variation in COL4A1/COL4A2 is associated with sporadic cerebral small vessel disease. *Neurology*. 2015;84:918–926.

51. Rannikmäe K, Sivakumaran V, Millar H, Malik R, Anderson CD, Chong M, Dave T, Falcone GJ, Fernandez-Cadenas I, Jimenez-Conde J, Lindgren A, Montaner J, O'Donnell M, Paré G, Radmanesh F, Rost NS, Slowik A, Söderholm M, Traylor M, Pulit SL, Seshadri S, Worrall BB, Woo D, Markus HS, Mitchell BD, Dichgans M, Rosand J, Sudlow CLM, Stroke Genetics Network (SiGN), METASTROKE Collaboration, and International Stroke Genetics Consortium (ISGC). COL4A2 is associated with lacunar ischemic stroke and deep ICH: Meta-analyses among 21,500 cases and 40,600 controls. *Neurology*. 2017;89:1829–1839.

FIGURES and LEGENDS

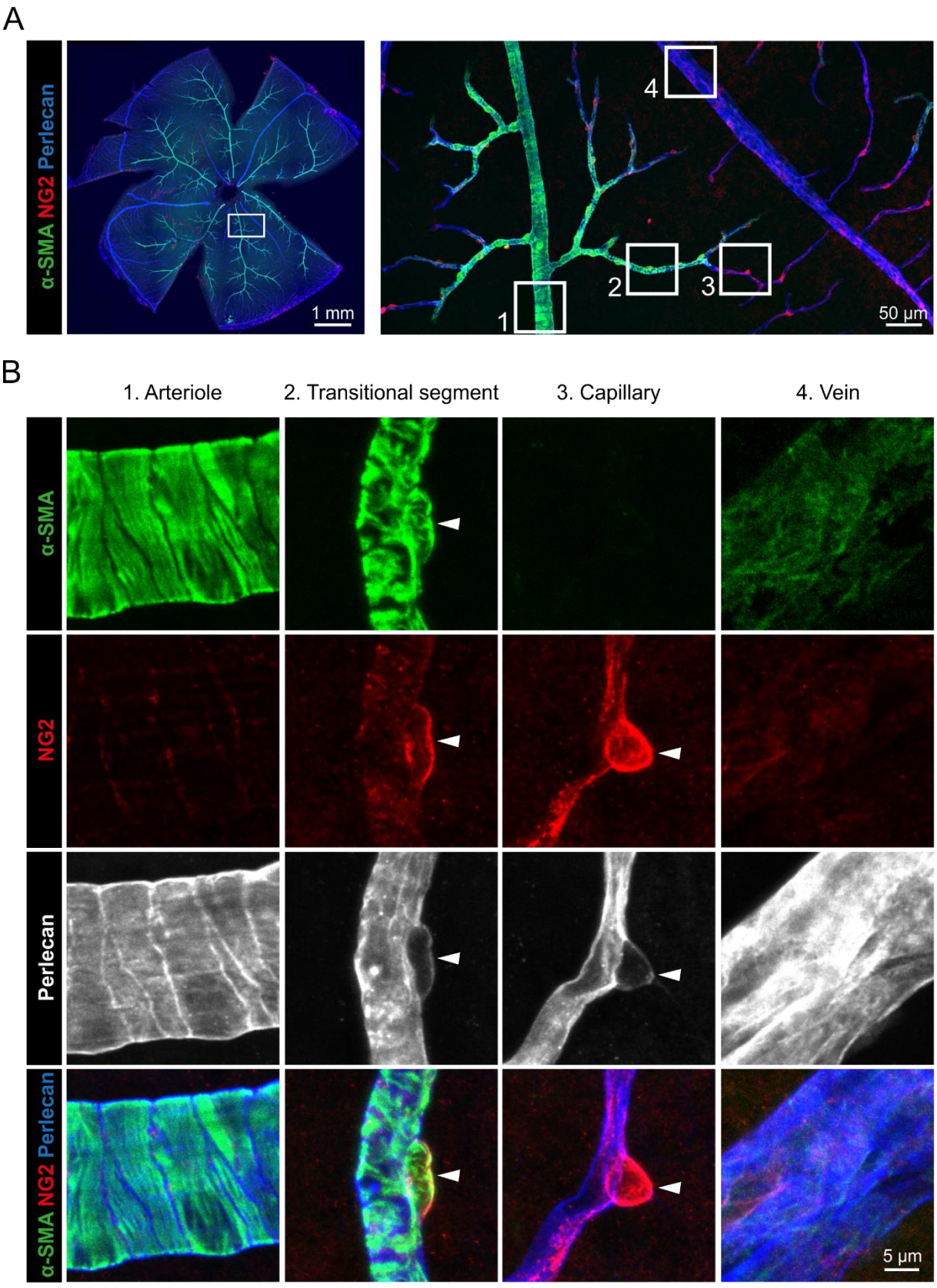

Figure 1

Figure 1. Heterogeneity of mural cells in retinal vessels. Confocal pictures of adult mouse retina immunostained for α-SMA, NG2 and perlecan. **A**. Whole flat mounted retina (left panel). Higher magnification of the boxed region (right panel). **B**. Higher magnification pictures of the boxed regions numbered in A, showing SMCs in arterioles (1), transitional cells in transitional segments (2), pericytes in capillaries (3) and SMCs in veins (4). Arrowheads show protruding cell body in transitional segments and capillaries. Scale bars: 1 mm (A, left), 50 µm (A, right) and 5 µm (B).

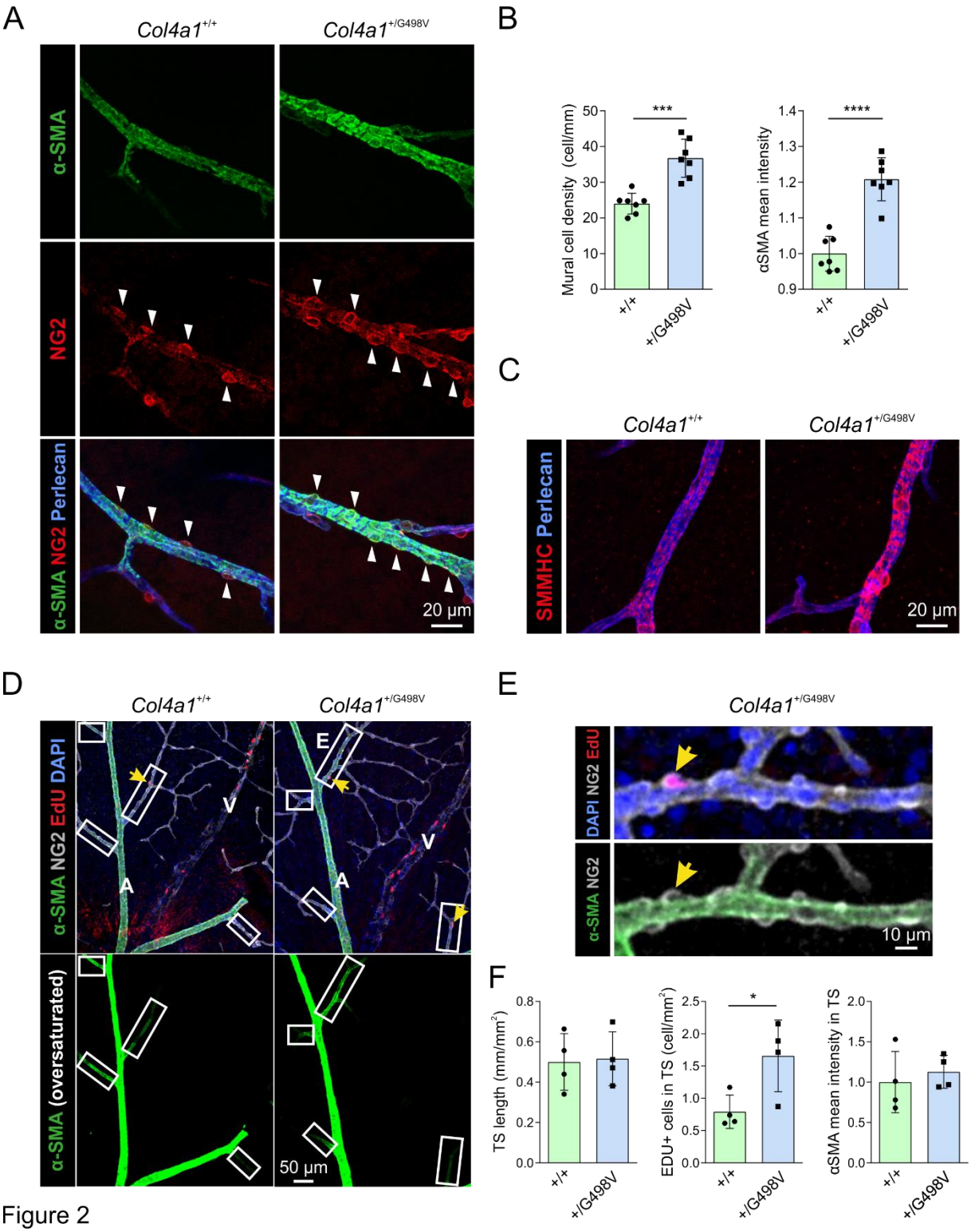

Figure 2

Figure 2. TS in *Col4a1*$^{+/G498V}$ retina are hypermuscularized in adult mice and exhibit increased mural cell proliferation during the post-natal maturation of the retinal vasculature. A. Representative confocal pictures of retinal TS from *Col4a1*$^{+/+}$ and

Col4a1$^{+/G498V}$ mice aged 6 months stained for α-SMA, NG2 and perlecan. TS in mutant mice exhibit greater α-SMA fluorescence intensity and an increased number of transitional cells (arrowheads). **B**. Quantification of mural cell density and α-SMA mean fluorescence intensity in retinal TS of *Col4a1*$^{+/+}$ and *Col4a1*$^{+/G498V}$ mice at 6 months (n=7 mice per group). *** P=0.0001 **** P<0.0001 by Student's t-test. **C**. Representative confocal pictures of TS of *Col4a1*$^{+/+}$ and *Col4a1*$^{+/G498V}$ mice at 6 months stained for SMMHC and perlecan showing higher SMMHC expression in mutant vessels. **D.** Representative confocal images of retinal arterioles (A) and TS (white boxes) of *Col4a1*$^{+/+}$ and *Col4a1*$^{+/G498V}$ mice aged 10 days, stained for EdU incorporation (4 hours) together with α-SMA, NG2, and DAPI— Shown are oversaturated images of α-SMA staining to better visualize TS (bottom panel). Yellow arrows depict proliferating mural cells in TS. Note the sustained cell proliferation in wildtype and mutant veins (V). **E.** Higher magnification views of the boxed area in D showing a proliferating mural cell in the TS of a *Col4a1*$^{+/G498V}$ mouse (yellow arrow) **F**. Quantification of the total length of TS (P=0.8746) stained by α-SMA, mural cell proliferation in TS (* P=0.0298) and α-SMA mean fluorescence intensity in TS (P=0.5753). Data were analyzed by Student's t-test (n=4 mice per group). Scale bars: 20 μm (A, C), 50 μm (D) and 10 μm (E).

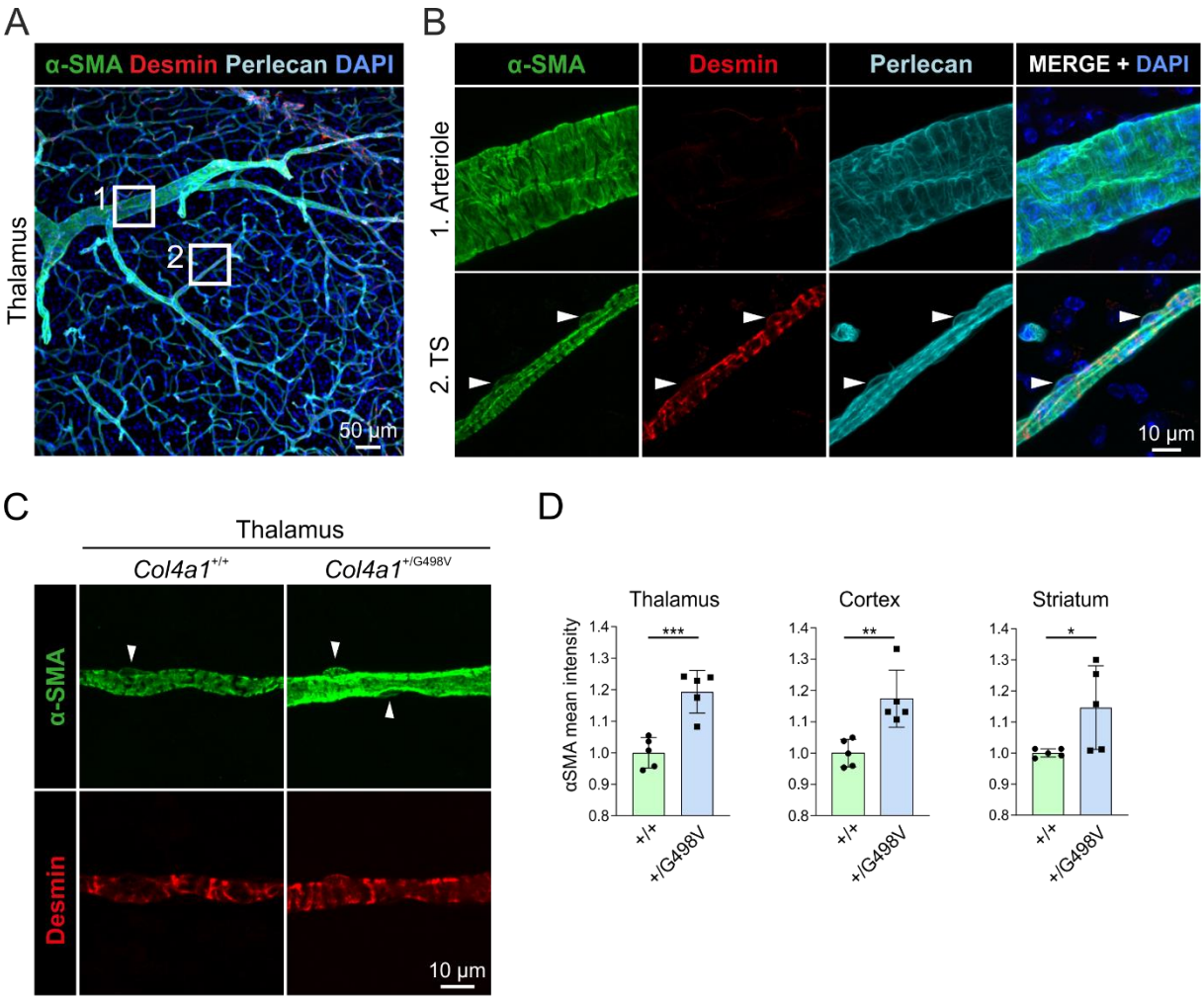

Figure 3

Figure 3. TS are present in the brain vasculature and are hypermuscularized in *Col4a1*$^{+/G498V}$ mice. A, B Representative confocal pictures of an adult wildtype mouse brain immunostained for α-SMA, desmin, perlecan and Dapi. **A**. Low magnification view of a vascular tree. **B**. Higher magnification pictures of the boxed regions numbered in A, showing SMCs in arterioles (1), and transitional cells in TS (2). Arrowheads point to the protruding cell body of transitional cells in the TS, containing the nucleus. **C**. Representative confocal pictures of TS in the thalamus from *Col4a1*$^{+/+}$ and *Col4a1*$^{+/G498V}$ mice aged 6 months stained for α-SMA and desmin, showing increased α-SMA immunoreactivity in mutant TS. Arrowheads point to cell nucleus of transitional cells. **D**. Quantification of α-SMA mean fluorescence intensity in TS of *Col4a1*$^{+/+}$ and *Col4a1*$^{+/G498V}$ mice aged 6 months in the

thalamus (*** P=0.0008), cortex (** P=0.005) and striatum (* P=0.0422). Data were analyzed by Student's t-test (n=5 mice per group). Scale bars: 50 µm (A) and 10 µm (B,C).

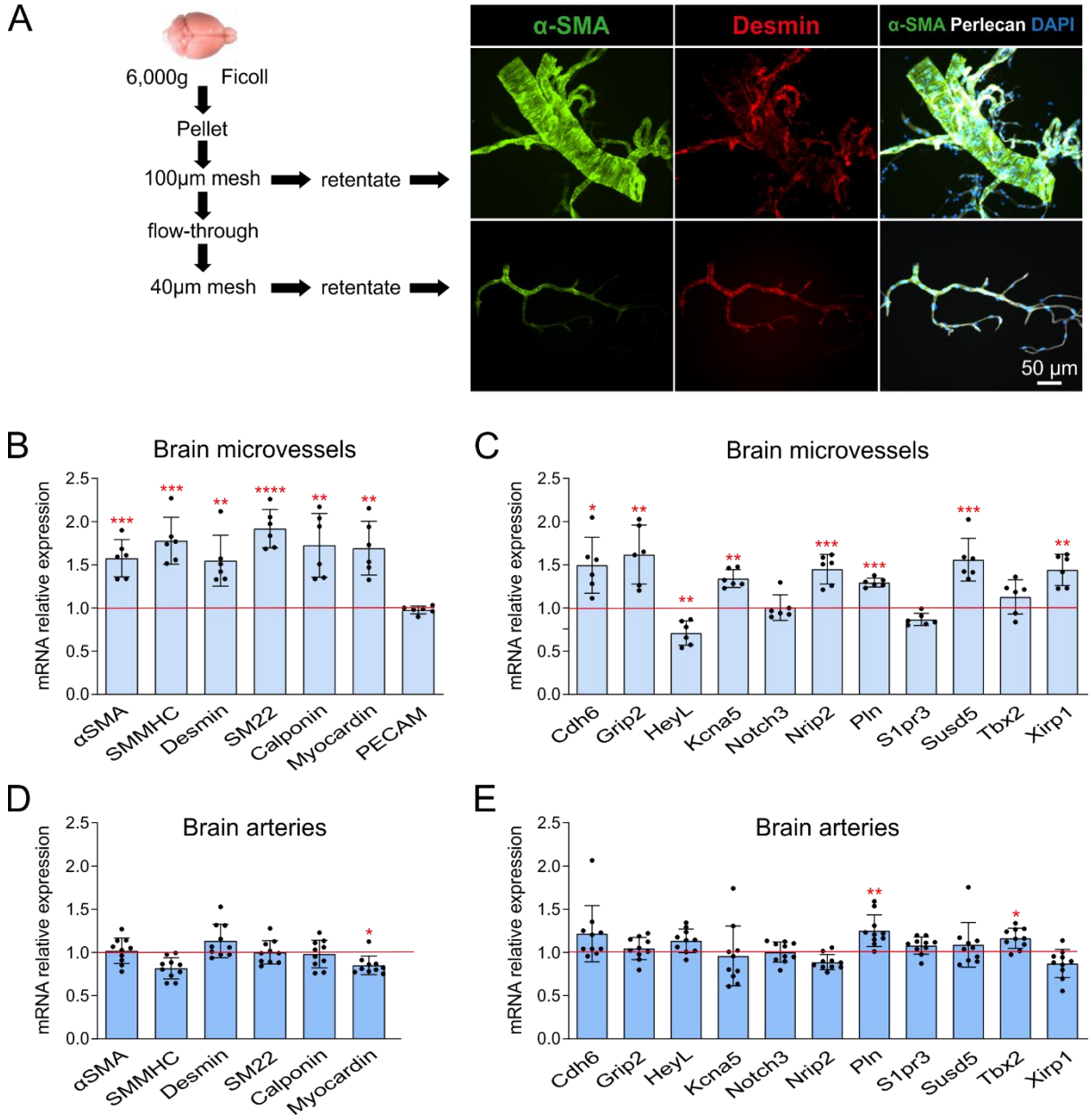

Figure 4

Figure 4. Gene expression level of SMC genes and Notch3 target genes in brain microvessels and brain arteries of *Col4a1*$^{+/+}$ and *Col4a1*$^{+/G498V}$ mice. A. Microvessels were prepared from mouse brain by homogeneization and centrifugation into Ficoll solution as described in the supplementary method section. Vessel preparations were then fractionated successively through 100 and 40 µm nylon meshes. Pictures show vessels retained on each nylon mesh (100 and 40 µm-fractions) stained for α-SMA, desmin, perlecan and DAPI. Arterioles (bright for α-SMA and low for desmin) were retained in the 100 µm-fraction and

40 µm-fractions were enriched in TS (bright for α-SMA and desmin) and capillaries. **B, C**. Relative mRNA levels of smooth muscle genes (**B**) and Notch3 target genes (**C**) measured by quantitative RT-PCR on 40 µm-fractions prepared from *Col4a1*$^{+/+}$ and *Col4a1*$^{+/G498V}$ adult mice (n=6 mice per group). Data are reported as a fold change over control mice and analyzed by Student's t-test. α-SMA (*** *P*=0.0007), SMMHC (*** *P*=0.0002), Desmin (** *P*=0.0018), SM22 (**** *P*<0.0001), Calponin (** *P*=0.0041), Myocardin (** *P*=0.0013), PECAM (*P*=0.4934), Cdh6 (* *P*=0.0117), Grip2 (** *P*=0.0048), HeyL (** *P*=0.0035), Kcna5 (** *P*=0.0060), Notch3 (*P*=0.9697), Nrip2 (*** *P*=0.0002), Pln (*** *P*=0.0007), S1pr3 (*P*=0.0530), Susd5 (*** *P*=0.001), Tbx2 (*P*=0.1972), and Xirp1 (** *P*=0.0085). **D, E**. Relative mRNA levels of smooth muscle genes (**D**) and Notch3 target genes (**E**) measured by quantitative RT-PCR in dissected brain arteries from *Col4a1*$^{+/+}$ and *Col4a1*$^{+/G498V}$ adult mice (n=10 mice per group). Data are reported as a fold change over control mice and analyzed by Student's t-test. α-SMA (*P*=0.7811), SMMHC (*P*=0.0506), Desmin (*P*=0.1680), SM22 (*P*=0.9903), Calponin (*P*=0.8291), Myocardin (* *P*=0.0407), Cdh6 (*P*=0.0609), Grip2 (*P*=0.5982), HeyL (*P*=0.1397), Kcna5 (*P*=0.8060), Notch3 (*P*=0.9669), Nrip2 (*P*=0.1677), Pln (** *P*=0.0062), S1pr3 (*P*=0.4643), Susd5 (*P*=0.4996), Tbx2 (* *P*=0.0309), and Xirp1 (*P*=0.2664). Scale bar: 50 µm (A).

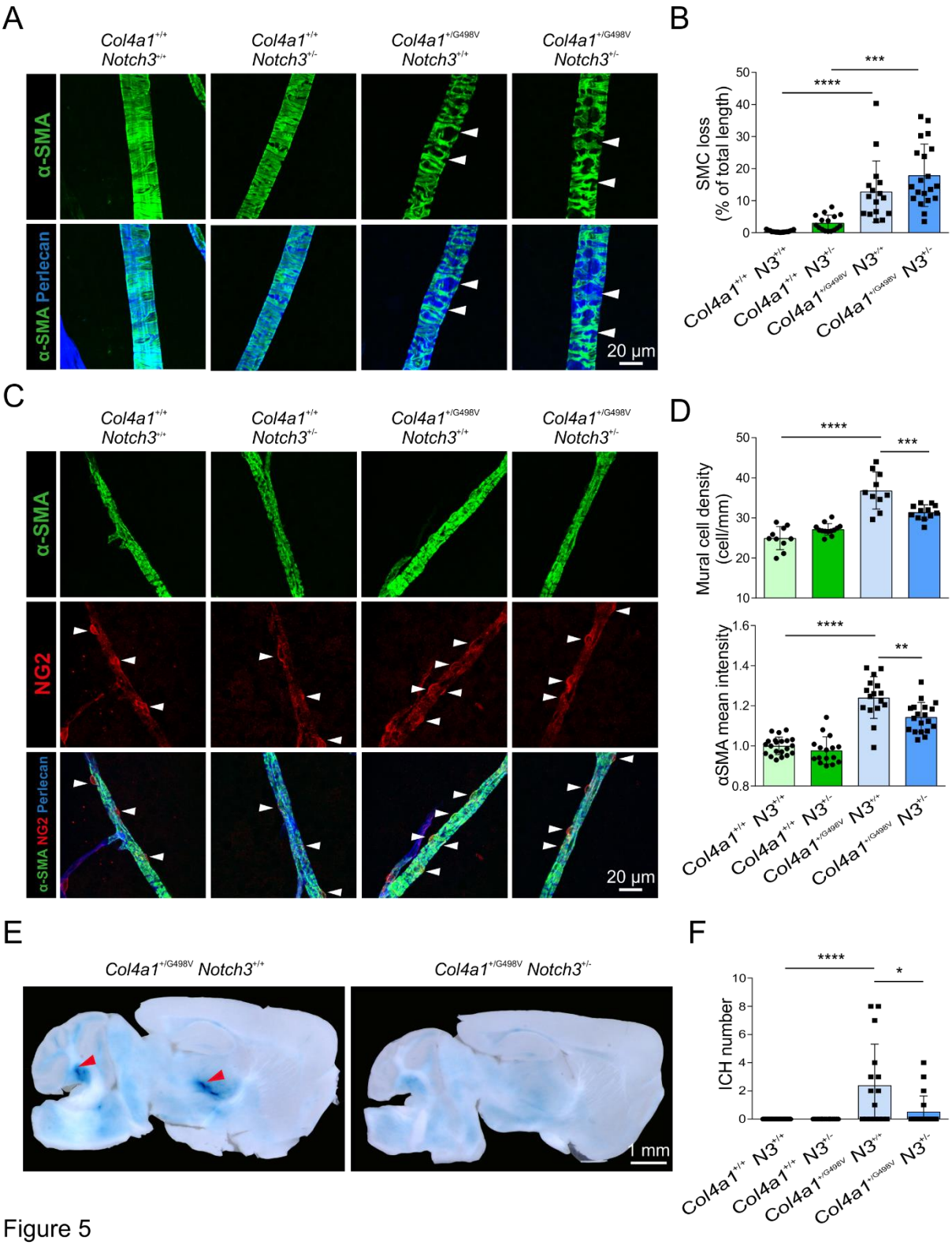

Figure 5

1

2 **Figure 5. Genetic reduction of Notch3 attenuates the hypermuscularization of TS in the**

3 **retina and protects *Col4a1* mutant mice against ICH.** *Col4a1*$^{+/G498V}$ mice were crossed

with *Notch3*$^{+/-}$ mice and issued mice of the four following genotypes were screened for microvascular lesions and ICHs at 6 months of age: *Col4a1*$^{+/+}$, *Notch3*$^{+/+}$; *Col4a1*$^{+/+}$, *Notch3*$^{+/-}$; *Col4a1*$^{+/G498V}$, *Notch3*$^{+/+}$ and *Col4a1*$^{+/G498V}$, *Notch3*$^{+/-}$. **A**. Representative confocal pictures of retinal arterioles stained for α-SMA and perlecan, showing SMC loss (arrowheads). **B**. Quantification of SMC loss in retinal arterioles showing no significant difference between *Col4a1*$^{+/G498V}$, *Notch3*$^{+/+}$ and *Col4a1*$^{+/G498V}$, *Notch3*$^{+/-}$ mice (from left to right n=21, 16, 16 and 20 mice). Data were analyzed with Kruskal-Wallis and Dunn's post-hoc test. *** P=0.0005 **** $P < 0.0001$. **C**. Representative confocal pictures of retinal TS stained for α-SMA, NG2 and perlecan. Arrowheads show cell bodies of transitional cells. **D**. Quantification of mural cell density (from left to right n=10, 13,10 and 12 mice) and α-SMA mean fluorescence intensity (from left to right n=21, 16,16 and 20 mice) in TS showing a significant reduction in mural cell density and α-SMA intensity in *Col4a1*$^{+/G498V}$ *Notch3*$^{+/-}$ mice compared to *Col4a1*$^{+/G498V}$ *Notch3*$^{+/+}$ mice. Data were analyzed by one-way ANOVA and Tukey's post-hoc test. Mural cell density *** P=0.0004 ,**** P<0.0001. α-SMA intensity **** P<0.0001. **E.** Representative images of sagittal brain sections stained for hemosiderin. Arrowheads depict deep ICHs. **F**. Quantification of the number of ICH showing a significant decrease in ICH number in *Col4a1*$^{+/G498V}$, *Notch3*$^{+/-}$ mice compared to *Col4a1*$^{+/G498V}$, *Notch3*$^{+/+}$ mice (from left to right n=21, 16,16 and 20 mice). Data were analyzed by Kruskal-Wallis and Dunn's post-hoc test. * P=0.020, **** P<0.0001. Scale bars: 20 µm (A, C) and 1 mm (E).

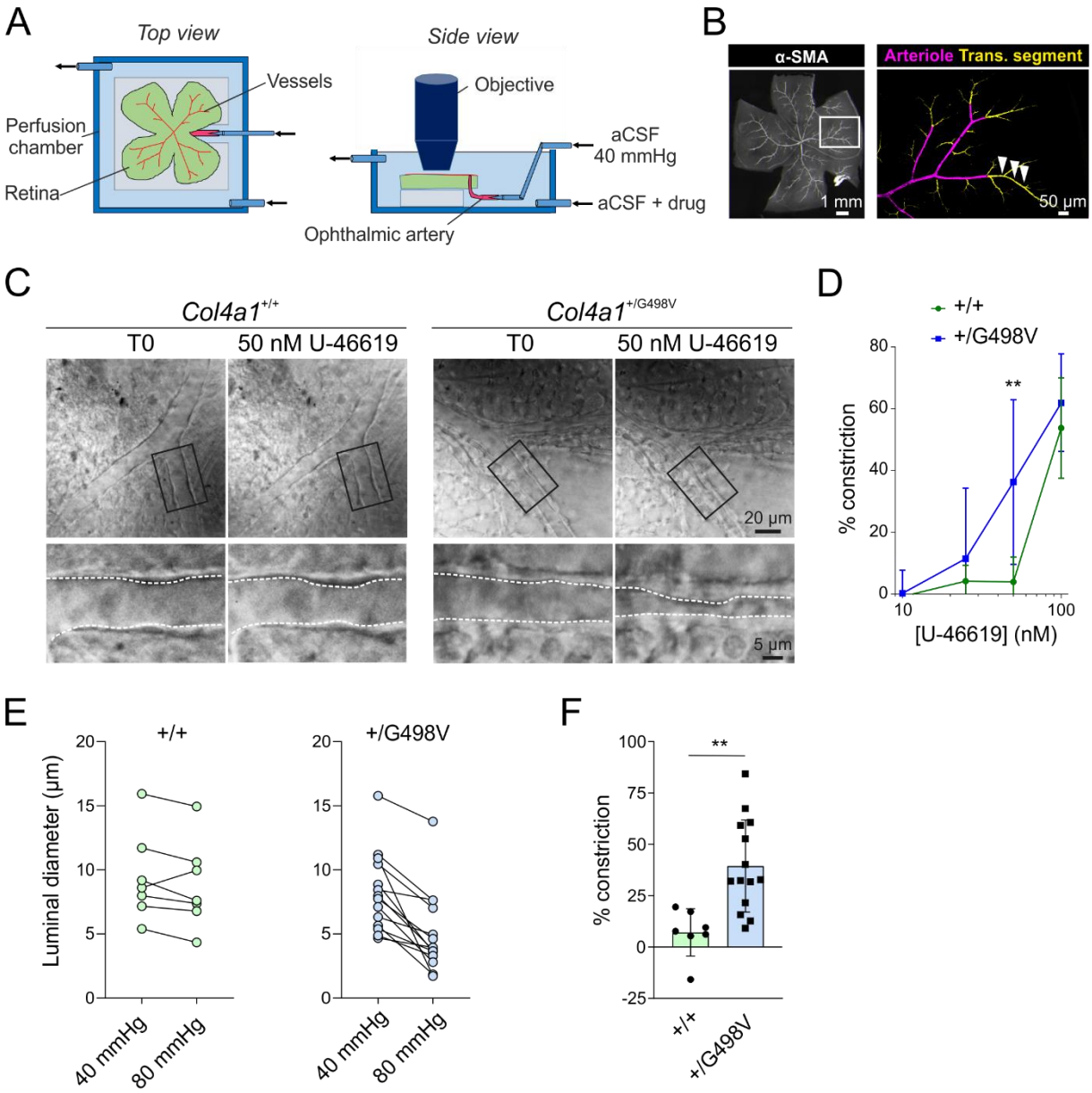

Figure 6

Figure 6. Agonist and pressure-induced contractile responses are greater in TS of *Col4a1*$^{+/G498V}$ mice. A. Experimental setup to analyze contractility and tone of the TS in retina explants. The retina was dissected with the ophthalmic artery and pinned on a silicon platform with the vessels facing upwards and immerged in a perfusion chamber filled with circulating aCSF at 37°C. To pressurize retinal vessels, ophthalmic artery was cannulated on a micropipette fed with a gravity column of CSF at 40 mmHg. Changes in vessel diameters were observed using a water immersion 40X objective. **B**. Whole retina (left panel).

Schematic depicting TS (yellow, arrowheads) and arterioles (purple) analyzed in these experiments (right panel)— noting that the capillaries are not depicted in this schematic. **C**. Differential interference contrast images of TS from *Col4a1*$^{+/+}$ and *Col4a1*$^{+/G498V}$ mice aged 6 months before (T0) and after addition of 50 nM thromboxane agonist U-46619 to the perfusion chamber. Bottom pictures show higher magnification view of boxed regions. Dashed white lines delineate the vessel wall. **D**. Dose response curve showing increased constriction of *Col4a1*$^{+/G498V}$ TS in response to U-46619 (n=5 *Col4a1*$^{+/+}$ and 9 *Col4a1*$^{+/G498V}$ mice). **E.** Decreasing diameters of individual TS following 40 mmHg to 80 mmHg pressure increase at the ophthalmic artery **F.** Increased pressure-induced constriction in *Col4a1*$^{+/G498V}$ TS, shown as percent constriction (relative to 40 mmHg diameter, n=7 vessels from 3 *Col4a1*$^{+/+}$ mice and n=14 vessels from 5 *Col4a1*$^{+/G498V}$ mice). Data were analyzed by repeated measure 2-way ANOVA and Bonferroni's multiple comparison test (panel D, ** P=0.0051), or Student's t-test (panel F, ** P=0.0021). Scale bars: 1mm (B, left), 50 µm (B, right), 20 µm (C, top) and 5 µm (C, bottom).

A

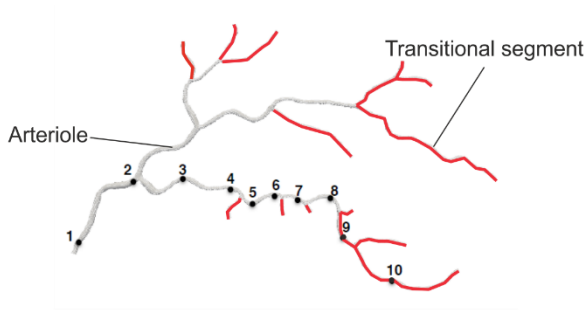

B

	Wild-type	*Col4a1*$^{+/mut}$	*Notch3*$^{-/-}$
Systolic pressure at entry of retinal network (mmHg)	45	40	45
Diastolic pressure at entry of retinal network (mmHg)	40	35	40
Density of SMCs in arterioles	1	0.85	0.85
Density of mural cells in transitional segments	1	1.25	0.85

C

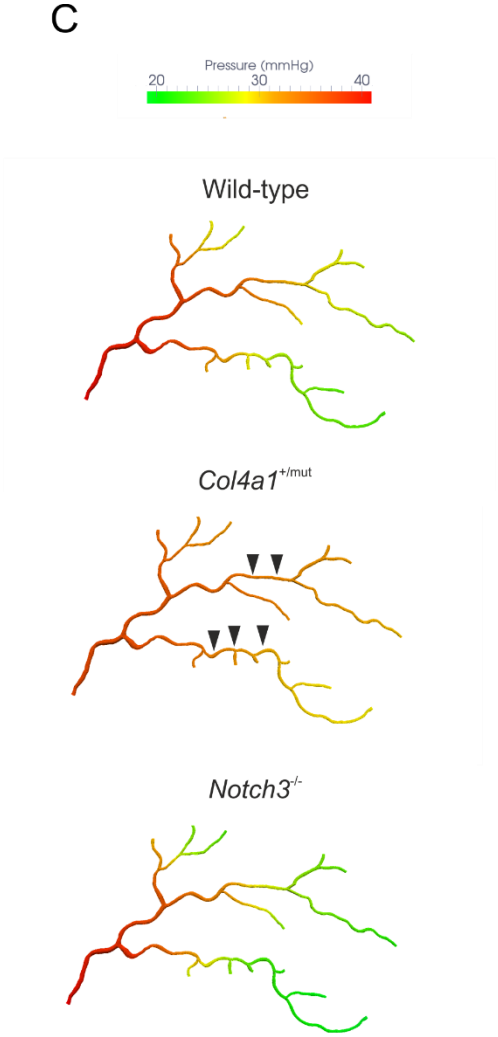

D

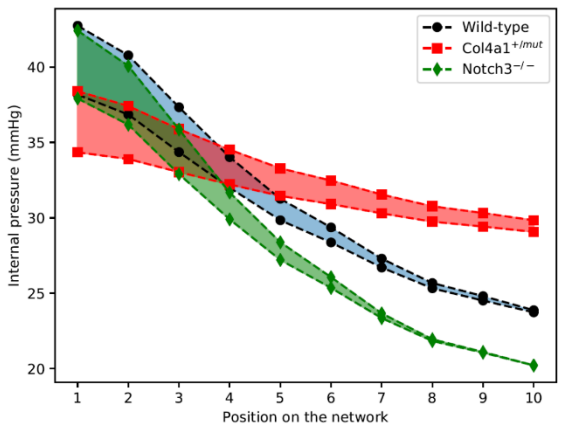

E

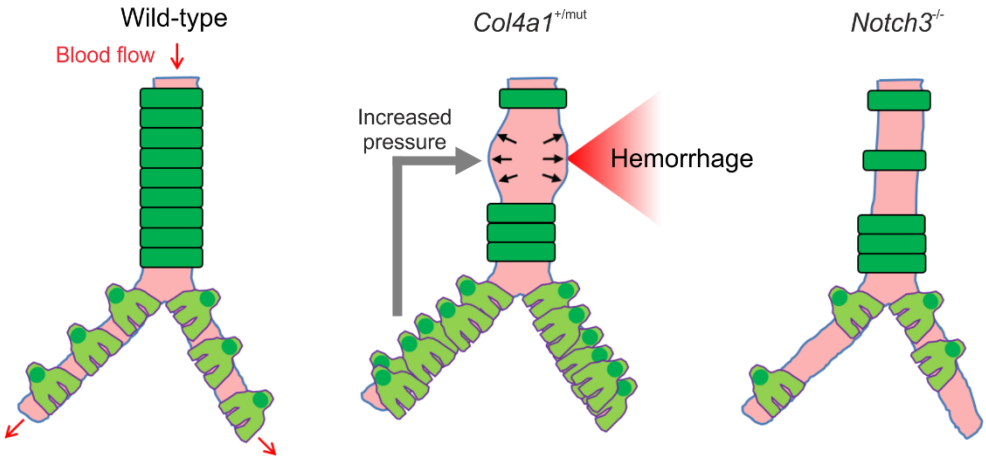

1 Figure 7

Figure 7. Computational modeling predicts that excessive muscularization of the TS increases intravascular pressure in the upstream arteriolar segment. A. Geometry of the human retinal vascular tree used for mathematical modeling. Arterioles are depicted in grey and transitional segments in red. **B**. Input parameters used for mathematical modeling. **C**. Color-coded representation of systolic intravascular pressures along the retinal vascular tree simulated with the model in wild-type (top), *Col4a1* mutant (middle) and *Notch3*$^{-/-}$ (bottom) mice, showing that pressure is elevated in terminal arterioles and TS of *Col4a1* mutant mice (arrowheads) but reduced in *Notch3*$^{-/-}$ mice. **D**. Graph showing simulated systolic and diastolic pressures at 10 different points on the vascular tree represented in A. **E**. Proposed working model of the mechanism of arteriolar wall rupture in *Col4a1* mutant mice.

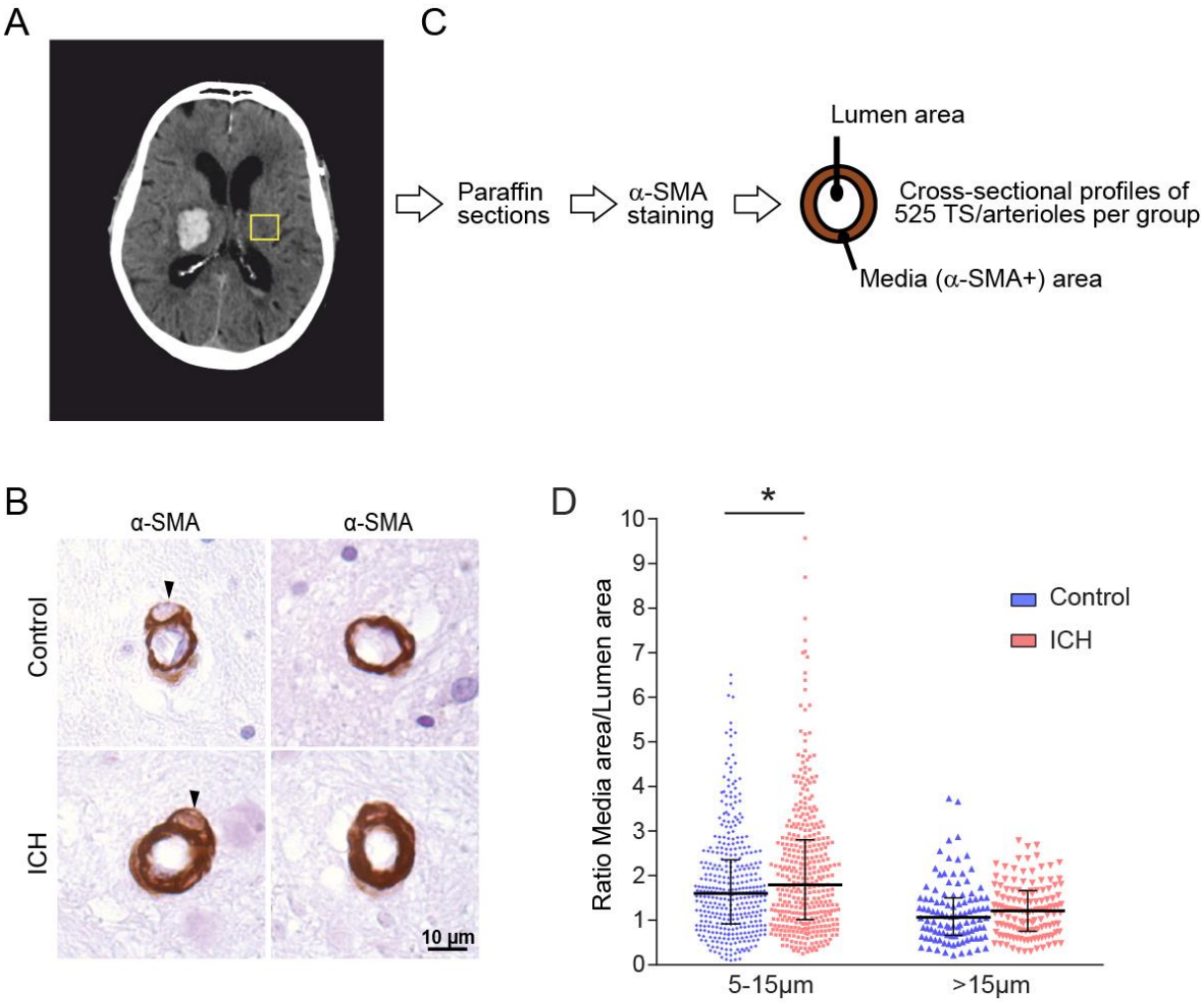

Figure 8

Figure 8. Hypermuscularization of the TS in humans with deep ICH. A. Representative image of a CT-scan showing a deep ICH in the left thalamus. Brain tissue was sampled after death in the contralateral basal ganglia for immuno-histochemistry (boxed region) and embedded in paraffin. **B**. Representative images of cerebral TS (basal ganglia) stained for α-SMA showing an hypermuscularization in ICH patients. Arrowheads point to transitional cell bodies. **C**. Schematic of the methodology used to quantify vessel wall remodeling. Cross-sectional profiles of 525 randomly selected arterioles/TS were analyzed in each group. **D**. Ratio of the vessel area stained for α-SMA (media) over the area of the lumen in cerebral

arterioles/TS from control and ICH patients. Vessels were stratified into two categories according to their lumen diameter (5 to 15 µm, TS and > 15 µm, arterioles). From left to right n = 368 and 382 TS (5-15µm), 106 and 128 arterioles (>15µm) analyzed. Data are presented as scatter plots with median value and first/third quartiles. Data were analyzed by Kruskal-Wallis and Dunn's post-hoc test. * *P*=0.016 Scale bar: 10 µm (B).